Nonlinear Dyn (2018) 92:793–802
https://doi.org/10.1007/s11071-018-4061-0

ORIGINAL PAPER

Research of giant magnetostrictive actuator's nonlinear dynamic behaviours

Xiaohui Gao · Yongguang Liu

Received: 13 March 2017 / Accepted: 5 January 2018 / Published online: 26 March 2018

Abstract The multi-coupled nonlinear factors existing in the giant magnetostrictive actuator (GMA) have a serious impact on its output characteristics. If the structural parameters are not properly designed, it is easy to fall into the nonlinear instability, which has seriously hindered its application in many important fields. The electric–magnetic-machine coupled dynamic mathematical model for GMA is established according to J-A dynamic hysteresis model, ampere circuit law, nonlinear quadratic domain model and structure dynamics equation. Nonlinear dynamic analysis method is applied to study the nonlinear dynamic behaviour of the key structure parameters to reveal their influence on the system stability. The design principle of structural parameters is obtained by studying stability of GMA, which provides theoretical basis and technical support for the structural stability design.

Keywords GMA · J-A model · Nonlinear dynamic behaviours · Stability

1 Introduction

Since the 1970s, giant magnetostrictive material (GMM) has developed very rapidly as a kind of strategic functional material. It has been widely applied in active vibration isolation, precision control, transducer and many other fields because of its high energy conversion efficiency, large output displacement and good dynamic characteristics [1–3]. But, it is very easy to fall into the nonlinear instability in high frequency because of strong multiple nonlinear factors [4–6]. The existence of nonlinear instability and even chaotic phenomena in GMA makes it difficult to predict and control, which seriously hinders its application in many important fields. James, Lei Wang, William S and Mao Jianqin applied robust control [7], self-adaptive control algorithm [8], optimal control [9] and H∞ control [10] to reduce the influence of nonlinear factors and improve the tracking accuracy and stability of GMA. The research of GMA structural design is mainly about reducing magnetic flux leakage and improving the magnetic field [11,12]. So far, researches about how to improve the stability of GMA are mainly done in the control strategies, while there are no deep studies on the reason of nonlinear instability and the structural stability design severely lacks theoretical guidance. Therefore, this paper firstly establishes the electric–magnetic–machine coupled model and then applies bifurcation diagram, Poincaré map, time-domain waveform, phase diagram and spectral analysis to analyse the GMA nonlinear dynamics behaviour characteristics. Finally, the design principles of structural parameters based on stability are achieved and proved in experiment.

X. Gao · Y. Liu (✉)
School of Automation Science and Electrical Engineering, Beihang University, No.37 Xueyuan road, Haidian district, Beijing 100191, People's Republic of China
e-mail: lyg@buaa.edu.cn

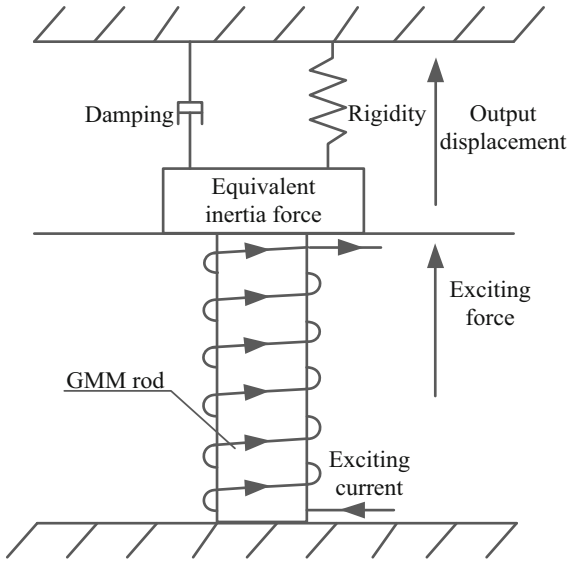

Fig. 1 Equivalent model of GMA

2 GMA model

GMA can be seen as a second-order quality-elastic-damping system with one degree of freedom according to its working principle. The equivalent mechanical model is shown in Fig. 1, and the dynamic equation is established according to Newton's second law.

$$F = -\sigma S = M_e\ddot{x} + C_e\dot{x} + F_z \tag{1}$$

$$M_e = \frac{M_M}{3} + M_L \tag{2}$$

where F is the output force of GMM rod, M_e is the equivalent mass, C_e is the equivalent damping coefficient, F_z is the restoring force of disc spring, whose computing method is in appendix A, S is the GMM rod's cross-sectional area, x is the output displacement of GMA, M_M is the mass of GMM rod, M_L is mass of the load.

$$x = \varepsilon L \tag{3}$$

where ε is the strain of GMM rod, and L is the length of GMM rod.

The quadratic moment domain rotation model is introduced into the linear piezomagnetic equation, and the nonlinear piezomagnetic equation is achieved [13].

$$\varepsilon = \sigma/E + \gamma_1 M^2 \tag{4}$$

where γ_1 is GMM rod's nonlinear magnetic elasticity coefficient, E is GMM's elasticity modulus, M is the magnetization intensity, which can be achieved by magnetic field intensity H. The relationship between H and M is described in appendix A.

According to the ampere circuit theorem considering the magnetic flux leakage, when the bias magnetic field is H_{bias}, the magnetic field strength H is

$$H = H_{\text{bias}} + k_{\text{coil}} I \tag{5}$$

where k_{coil} is the exciting coefficient.

The nonlinear dynamic model of GMA can be achieved by uniting Eqs. 1–5, which takes the current I as input and displacement x as output.

$$M_e\ddot{x} + C_e\dot{x} + K_{e3}x^3 - K_{e2}x^2 + K_{e1}x = F(I) \tag{6}$$

where $K_{e3} = K_{\text{spr3}}$, $K_{e2} = K_{\text{spr2}}$, $K_{e1} = K_{\text{spr1}} + \frac{ES}{L}$ are the equivalent stiffness coefficients, $F(I) = \gamma_1 ESM(I)^2$ is output force produced by GMM rod, $M(I)$ is the magnetization when input current is I.

3 Research of nonlinear dynamic behaviour in GMA

In order to study the dynamic behaviour of GMA, the dynamic equation firstly is normalized and then solved by Runge–Kutta. Qualitative analysis of nonlinear dynamics is applied to study GMA's nonlinear dynamic behaviour characteristics and reveal the influence of key structural parameters on the system stability.

When the dimensionless displacement $u = x/\gamma_0$ and time $\tau = \omega_0 t$ are introduced, Eq. 6 is converted to be Eq. 7, where $\gamma_0 = \sqrt{K_{e1}/K_{e3}}$, $\omega_0 = \sqrt{K_{e1}/M_e}$.

$$\ddot{u} + \varphi_1\dot{u} + u^3 - \varphi_2 u^2 + u = f_\varphi F(\Omega\tau) \tag{7}$$

where $\varphi_1 = C_e/\sqrt{M_e K_{e1}}$ is dimensionless damping coefficient, $\varphi_2 = K_{e2}/\sqrt{K_{e1}K_{e3}}$ is square stiffness coefficient, $f_\varphi = \sqrt{K_{e3}/K_{e1}^3}$ is coupling stiffness coefficient, and $\Omega = \omega/\omega_0$ is angular frequency.

The effects of sensitive parameters on the system stability are revealed by studying the dynamics characteristics for φ_1, φ_2 and f_φ, which provide the theoretical foundation for GMA structure design based on stability.

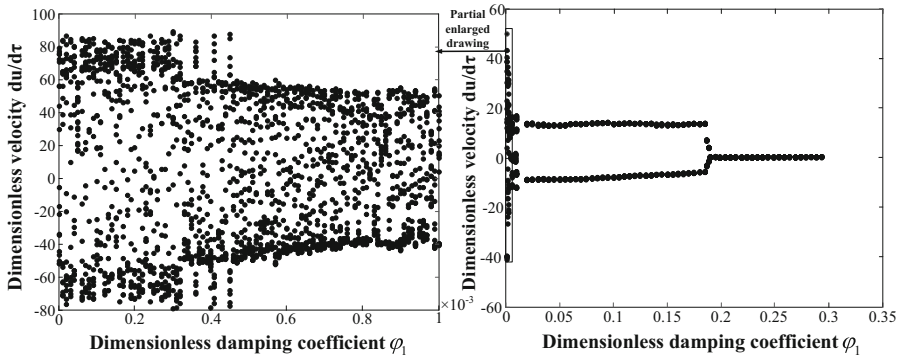

Fig. 2 Bifurcation diagram of φ_1

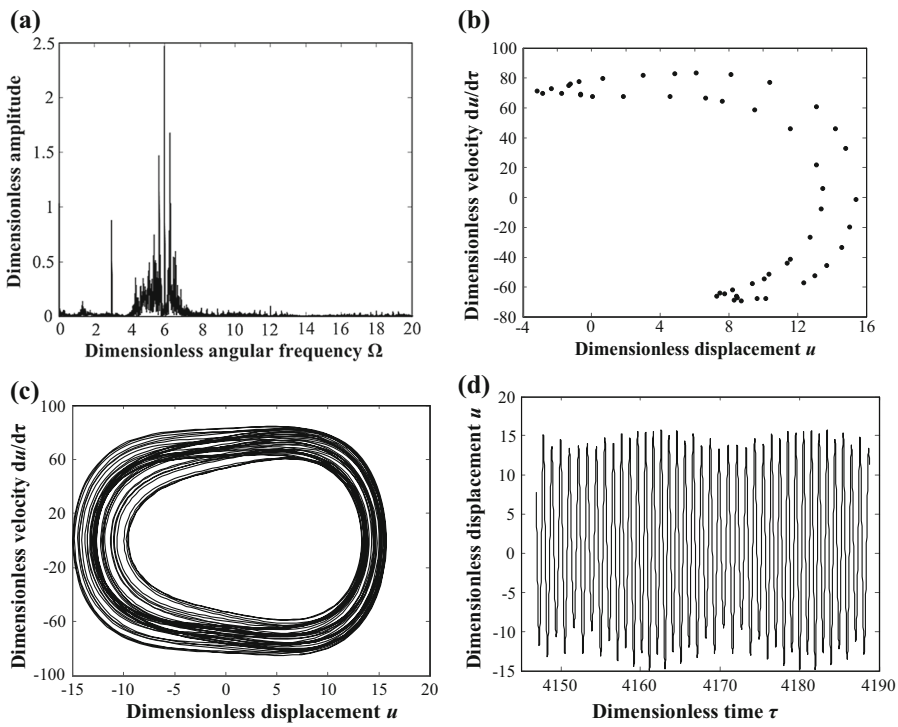

Fig. 3 Response characteristics in $\varphi_1 = 10^{-4}$. **a** Spectrum, **b** poincaré mapping, **c** phase diagram, **d** time-domain waveform

3.1 Research on the damping coefficient

Taking the dimensionless damping coefficient φ_1 as the reference variable, the bifurcation diagram is shown in Fig. 2 when $\Omega = 3$. The response characteristics are shown in Fig. 3 when $\varphi_1 = 10^{-4}$. Spectrum contains multi-frequency, Poincaré mapping is the distribution of random points in the global scope, phase diagram is composed of many circular curves without overlapping, and time-domain waveform is messy without periodicity, which indicates that system is in chaotic state. Figure 4 shows the response characteristics when $\varphi_1 = 0.15$. Spectrum shows that the main frequency is the integer times of 1/2 Ω and Poincaré mapping only has two points, which indicates that the system goes into period-doubling bifurcation. Figure 5 shows that the system is in the stable periodic motion when $\varphi_1 = 0.25$.

With the decrease of damping coefficient, system transforms from stable periodic motion, period-doubling bifurcation to chaos, which shows that smaller φ_1 can fall into the unstable chaotic state.

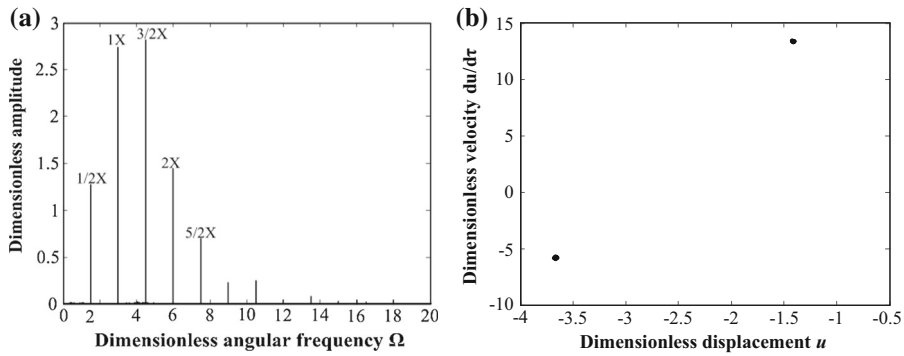

Fig. 4 Response characteristics in $\varphi_1 = 0.15$. **a** Spectrum, **b** poincaré mapping

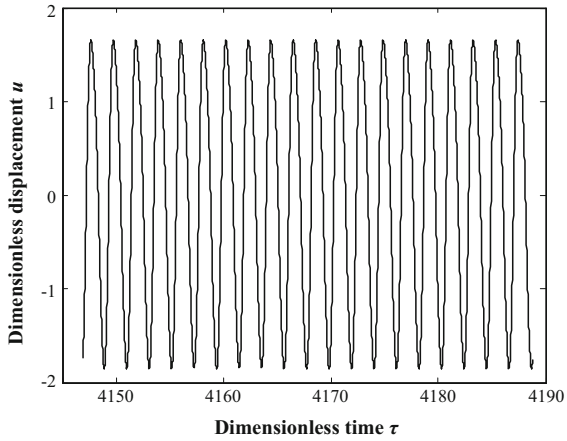

Fig. 5 Time-domain waveform in $\varphi_1 = 0.25$

3.2 Research on the square stiffness coefficient

Taking the dimensionless square stiffness coefficient φ_2 as the variable, the nonlinear dynamic behaviour characteristics of the GMA are studied when $\Omega = 2$ and $\Omega = 3$. It can be seen from Fig. 6 that the system maintains the same bifurcation characteristic when φ_2 varies from 0 to 1 under different Ω. Therefore, φ_2 has nothing to do with the dynamic behaviour in the GMA.

3.3 Research on the coupling stiffness coefficient

Taking the coupling stiffness coefficient f_φ as the variable, the bifurcation diagram is shown in Fig. 7. With the increase of f_φ, the system goes from stable period, period-doubling bifurcation to chaos, which indicates that the larger f_φ makes the system enter the unstable chaotic state.

4 Parameters design based on the stability

It is concluded from Sect. 3 that the larger φ_1 and smaller f_φ can improve the stability according to nonlinear dynamic behaviour characteristics of GMA. According to $\varphi_1 = C_e/\sqrt{M_e K_{e1}}$, larger C_e and smaller K_{e1} can increase φ_1. But, smaller K_{e1} leads to smaller

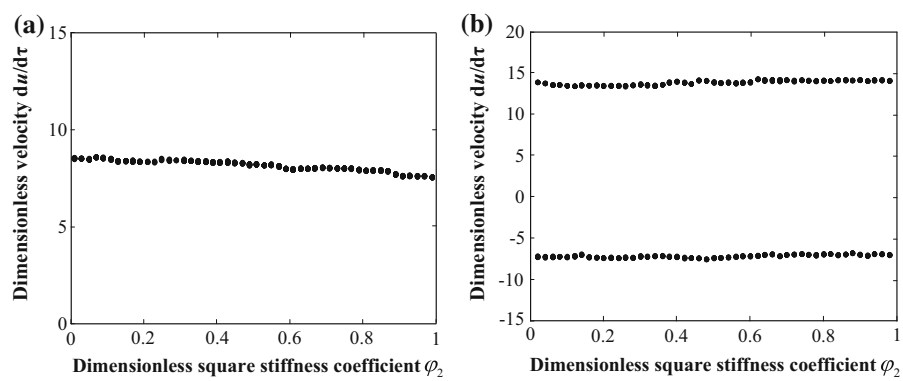

Fig. 6 Bifurcation diagram of φ_2. **a** $\Omega = 2$, **b** $\Omega = 3$

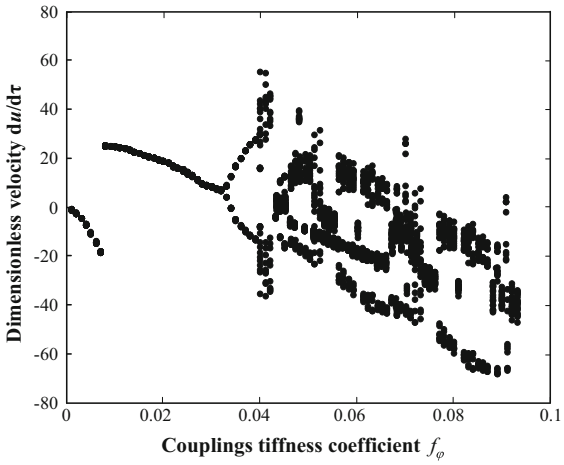

Fig. 7 Bifurcation diagram of f_φ

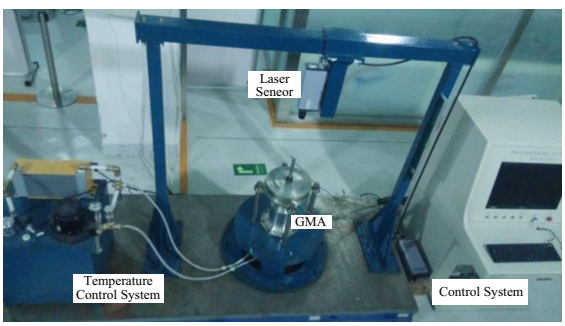

Fig. 8 GMA test bed

natural frequency $\omega_0 = \sqrt{K_{e1}/M_e}$. According to $f_\varphi = \sqrt{K_{e3}/K_{e1}^3}$, increasing K_{e1} and decreasing K_{e3} can decrease f_φ.Therefore, increasing C_e, K_{e1} and decreasing K_{e3} can improve the system stability.

According to $K_{e3} = K_{\text{spr3}}$, $K_{e1} = K_{\text{spr1}} + \frac{ES}{L}$ and disc spring characteristics in appendix A, the following conclusions can be drawn.

1. Increasing the GMM rod's S/L will increase K_{e1} and enhance the stability. So, slender GMM rod is not favourable for stability.
2. The coupling stiffness coefficient f_φ of A, B, C disc springs increases successively in the same diameter, and A disc spring has higher stability.
3. Increasing the diameter D of disc spring can increase K_{e1} and decrease K_{e3}, which can enhance the system stability.
4. The larger number of disc springs in overlap can reduce f_φ and improve stability, while the result of involution is just the opposite.

5 Test verification

GMA test bed (Fig. 8) is applied to do verification experiment for the mathematical model and stability. It is mainly composed of GMA, laser displacement sensor, temperature control system and control system. V100-MS laser displacement sensor can test the displacement of GMA, and its frequency response is up to 20 kHz. Temperature control system is applied to maintain a stable operating temperature for GMM rod. The diagram of control system is shown in Fig. 9. LabWindows and RTX are used for upper and lower computer, respectively, and sampling period is 0.5 ms. The control card in the industrial personal computer (IPC) sends the introductions to the servo drivers and then generates exciting current to activate GMA. The data acquisition card (DAQ) is used to achieve displacement through laser displacement. When doing some experiments, some experimental conditions must be satisfied.

1. The quiet working environment must be ensured, and any outside noise may affect the results.
2. The laser beam should be perpendicular to the cross section of output shaft in GMA. Otherwise, it will affect the measurement result.
3. Temperature control system should keep working in the experiment to maintain constant working temperature for GMM rod.

Fig. 9 Control system

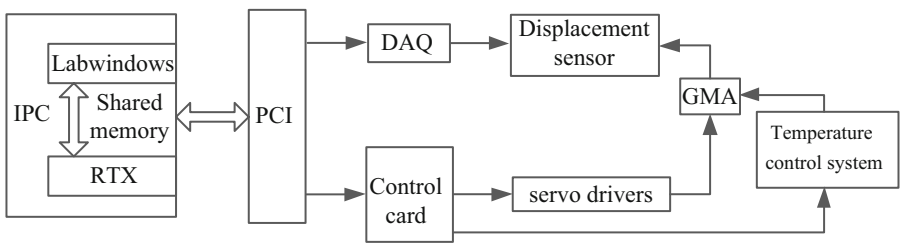

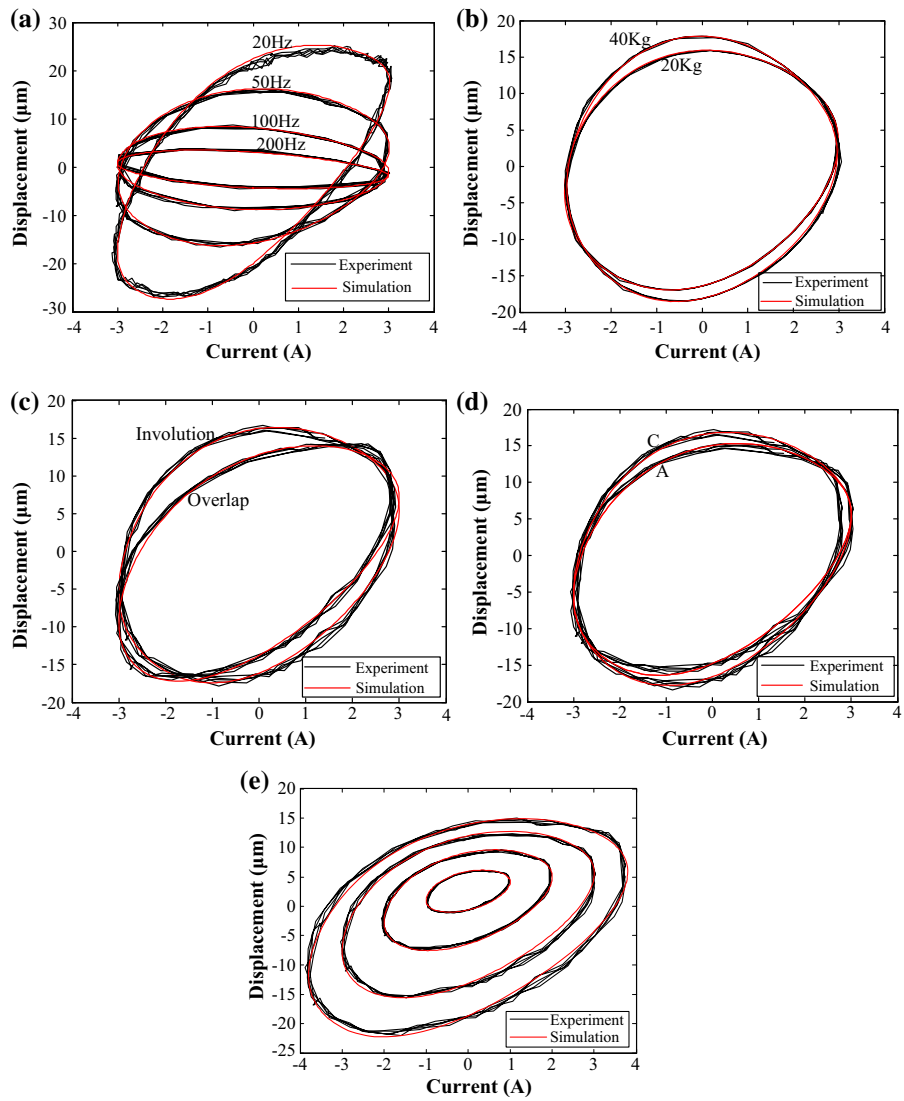

Fig. 10 Simulation and experiment. **a** Different frequency, **b** different loads, **c** different combination methods of disc springs, **d** different series of disc springs, **e** different minor loops

1. Mathematical model verification

Figure 10 is the simulation and experiment curve of GMA in different frequency, loads, combination methods, series of disc springs and minor loop. The good fitting proves the correctness and validity of the GMA model.

2. Stability verification

Figure 11 shows the spectrum of GMA output displacement in different structural parameters. When C disc springs are in involution and driving frequency is 166.7 HZ, the output displacement contains a variety of frequency, which indicates that the system is in chaos (Fig. 11a), while the system is in stable periodic motion when C disc springs are in overlap (Fig. 11b). When C disc springs are in overlap and driving frequency is 200 HZ, the system is in chaos (Fig. 11c), while the system is in stable periodic motion when it chooses A disc springs (Fig. 11d). Therefore, the higher structural stiffness can improve the stability of GMA.

6 Conclusion

1. Adding structural factors to the GMA mathematical model can effectively improve the accuracy of the model.

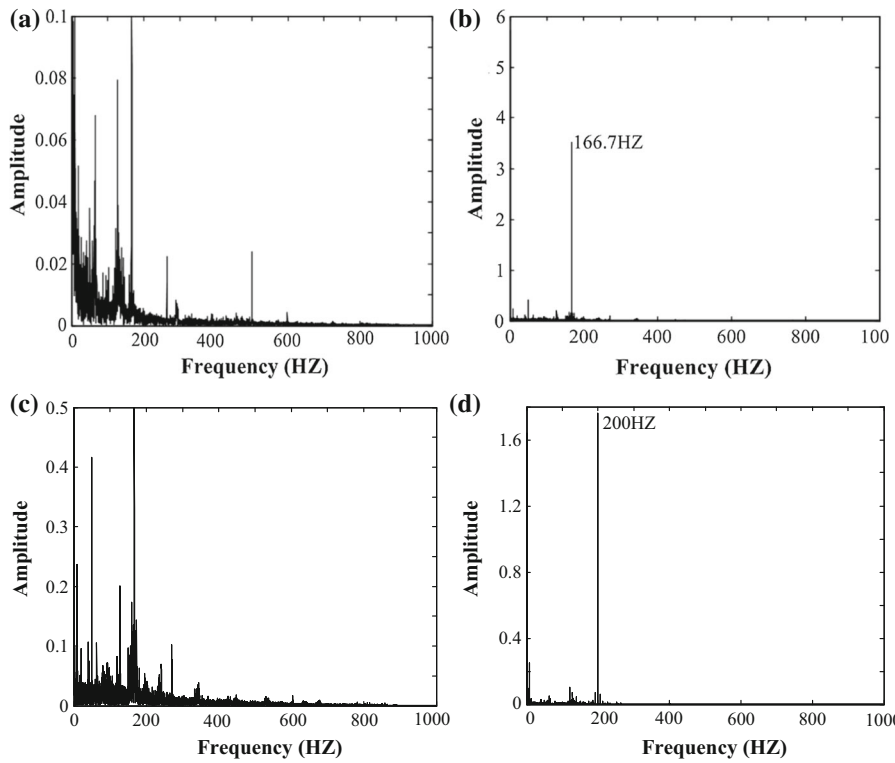

Fig. 11 Spectrum in different structural parameters. **a** Involution of C disc spring in 166.7 HZ, **b** overlap of C disc spring in 166.7 HZ, **c** overlap of C disc spring in 200 HZ, **d** overlap of A disc spring in 200 HZ

2. It is possible to cause the system to fall into instability with lower structure rigidity and damping.
3. Disc spring plays an important role in stability for GMA. The larger diameter D, higher number of n_c in overlap and A disc spring can effectively improve the stability

Acknowledgements This work was supported by the National Natural Science Foundation of China (11272026).

Appendix A

1. Working principles of GMA

The working principle of GMA is shown in Fig. 12. The GMM rod drives load under the action of the magnetic field generated by the excitation coil and permanent magnet. GMM needs pre-pressure produced by compacting disc spring to improve the magnetostriction coefficient. The ring permanent magnet can produce bias magnetic field to eliminate the double-frequency property of materials and export bidirectional displacement. Top and lower cover forms closed magnetic circuit to reduce magnetic leakage.

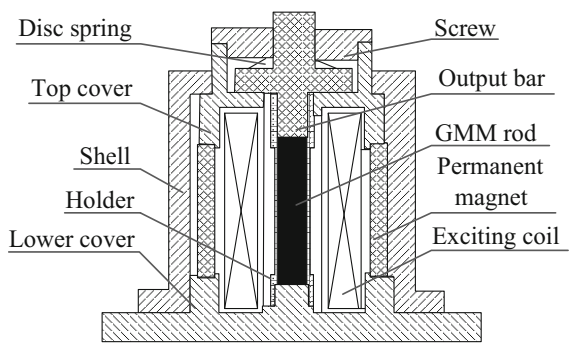

Fig. 12 GMA

2. GMM mode between H and M

Jiles–Atherton (J–A) model is established based on the magnetic wall motion theory existing in ferromagnetic material proposed by Jiles DC and Atherton DL and has developed into a relatively mature theory [14–18]. Classical J–A dynamic H–M model can be given as

$$H_e = H + \alpha M + \frac{9\lambda_s \sigma}{2\mu_0 M_s^2} M = H + \widetilde{\alpha} M \tag{A1}$$

$$M_{an} = M_s \left(\coth \frac{H_e}{a} - \frac{a}{H_e} \right) \tag{A2}$$

$$M = M_{rev} + M_{irr} \tag{A3}$$

$$M_{rev} = c(M_{an} - M_{irr}) \tag{A4}$$

$$M_{irr} = (M - cM_{an})/(1 - c) \tag{A5}$$

$$M = M_{an} - k\delta(1 - c)\frac{dM_{irr}}{dH_e} - k_1 \frac{dM}{dt}\frac{dM}{dH_e} - k_2 \left| \frac{dM}{dt} \right|^{\frac{1}{2}} \frac{dM}{dH_e} \tag{A6}$$

where H_e is the effective magnetic field intensity, H is the magnetic field intensity, M is the magnetization intensity, α is the average internal coupling field coefficient, σ is the stress on the GMM rod, μ_0 is the vacuum permeability, M_s is the saturation magnetization, λ_s is the saturation magnetostrictive coefficient, M_{an} is the anhysteretic magnetization, a is the shape parameter of anhysteretic magnetization, M_{rev} is the reversible magnetization, M_{irr} is the irreversible magnetization, c is the reversible loss coefficient, δ is the direction factor, when $dH/dt > 0$, $\delta = 1$ and when $dH/dt < 0$, $\delta = -1$, k is irreversible loss coefficient, k_1 is the eddy-current loss factor, and k_2 is anomalous loss factor.

The minor loop model can be got by modifying parameter a, α, c and k according to the parameters characteristics and the difference between simulation and experiment curves [19].

$$\begin{cases} a_{\min or} = a e^{\gamma_a(\lambda_s - \lambda_m)} \\ \alpha_{\min or} = \alpha e^{\gamma_\alpha(\lambda_s - \lambda_m)} \\ c_{\min or} = c e^{\gamma_c(\lambda_s - \lambda_m)} \\ k_{\min or} = k e^{\gamma_k(\lambda_s - \lambda_m)} \end{cases} \tag{A7}$$

where γ_k, γ_a, γ_c and γ_α are the local correction coefficients of k, a, c and α, respectively, $k_{\min or}$, $a_{\min or}$, $c_{\min or}$, $\alpha_{\min or}$ are the revised parameters of minor loop, and λ_m is the maximum magnetostrictive coefficient of minor loop.

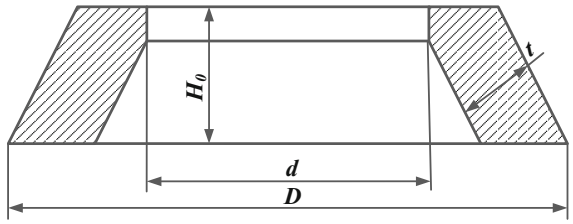

Fig. 13 Structure of disc spring

Table 1 Relationship between structure parameters of disc spring

Parameter	Parameter relationships
A	$D/t \approx 18$, $D/h_0 \approx 45$
B	$D/t \approx 28$, $D/h_0 \approx 37.3$
C	$D/t \approx 40$, $D/h_0 \approx 30.8$

3. Disc spring model

As the main device to exert pre-pressure on GMA, disc spring has an important influence on the output characteristics of GMA. The restoring force generated by the single disc spring is

$$F_d = K_{spr3} x_f^3 - K_{spr2} x_f^2 + K_{spr1} x_f \tag{A8}$$

where $K_{spr3} = \frac{t}{2\chi D^2}$, $K_{spr2} = \frac{3th_0}{2\chi D^2}$, $K_{spr1} = \frac{h_0^2 t + t^3}{\chi D^2}$, x_f is the disc spring deformation, and h_0 is the maximum deformation of disc spring . The structure of the disc spring is shown in Fig. 13.

According to literature 20, there are A, B and C series of disc springs and the relationship between D, t and h_0 is shown Table 1.

It can been seen from Table 1 that no matter what kind of disc spring it is, D/t and D/h_0 are constants. So, K_{spr3}, K_{spr2}, K_{spr1} are converted to Eq. A9.

$$\begin{cases} K_{spr1} = \frac{D}{\chi}\left(\frac{1}{C_t C_{h_0}^2} + \frac{1}{C_t^3} \right) \\ K_{spr2} = \frac{3}{2\chi C_t C_{h_0}} \\ K_{spr3} = \frac{1}{2\chi C_t D} \end{cases} \tag{A9}$$

where $D/t = C_t$, $D/h_0 = C_{h_0}$.

The disc spring also can change its structure stiffness by different combination methods (Fig. 14). Without considering the friction force between the disc springs, the calculation formula for the restoring force F_z and

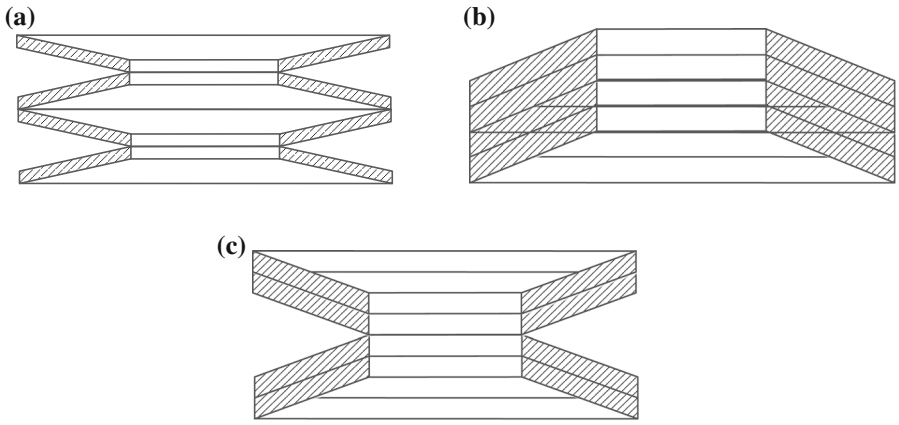

Fig. 14 Combination methods of disc springs. **a** Involution, **b** overlap, **c** mixture

Table 2 Characteristics in different combinations

Parameter	Restoring force	Deformation
Involution	$F_z = F_d$	$x = n_s x_f$
Overlap	$F_z = n_c F_d$	$x = x_f$
Mixture	$F_z = n_c F_d$	$x = n_s x_f$

Table 3 Model parameters

Parameter	Value	Parameter	Value
a	47704 A/m	k	22643 A/m
α	0.417	c	0.1
M_s	380769 A/m	k_2	0.312
k_{coil}	16492 m^{-1}	γ_1	1.07×10^{-14}
L	0.1 m	d	0.02 m
γ_a	-10	γ_α	10
γ_k	-30	γ_c	1500
H_{bias}	62669.6 A/m	λ_s	1500
k_1	5.89×10^{-5}	E	30 Gpa
M_M	291 g	μ_0	$4\pi \times 10^{-7}$ N/A^2
D	6.3 cm	χ	1.36×10^{-12}

total deformation x of the disc spring is shown in Table 2, where n_s and n_c are the number of disc springs in involution and overlap combination.

4. parameters

The model parameters for GMA are shown in Table 3 based on physical property and parameters identification [21].

References

1. Karunanidhia, S., Singaperumalb, M.: Design, analysis and simulation of magnetostrictive actuator and its application to high dynamic servo valve. Sens. Actuators A Phys. **157**(2), 185–197 (2010)
2. Zhang, H., Zhang, T., Jiang, C.: Magnetostrictive actuators with large displacement and fast response. Smart Mater. Struct. **21**, 1–7 (2012)
3. Yoshioka, H., Shinno, H., Sawano, H.: A newly developed rotary-linear motion platform with a giant magnetostrictive actuator. CIRP Ann. Manuf. Technol. **62**(1), 371–374 (2013)
4. Braghin, F., Cinquemani, S., Resta, F.: A low frequency magnetostrictive inertial actuator for vibration control. Sens. Actuators A Phys. **180**, 67–74 (2012)
5. Nakamura, Y., Nakayama, M., Masuda, K.: Development of active six-degrees-of-freedom microvibration control system using giant magnetostrictive actuators. Smart Mater. Struct. **9**(2), 175–185 (2000)
6. Feng, X., Zhang, H., Chengbao, J.: Designing and performance research of giant magnetostrictive actuator. Acta Aeronaut. Astronaut. Sin. **23**(6), 552–555 (2002)
7. James, R.C.S., Nealis, M.: Robust control of a magnetostrictive actuator. Proc. SPIE Int. Soc. Opt. Eng. **5049**, 221–232 (2003)
8. Wang, L., Tan, J.B., Liu, Y.T.: Research on Giant magnetostrictive micro-displacement actuator with self-adaptive control algorithm. J. Phys. Conf. Ser. **13**(1), 446–449 (2005)
9. Oates, W.S., Smith, R.C.: Nonlinear optimal control techniques for vibration attenuation using magnetostrictive actuators. J. Intell. Mater. Syst. Struct. **19**(2), 193–209 (2008)
10. Ping, L., Jianqin, M., Qingsong, L.: Modeling and H∞robust control for giant magnetostrictive actuators with rate-dependent hysteresis. Control Theory Appl. **30**(2), 148–155 (2013)
11. Xue, G., He, Z., Li, D.: Magnetic field intensity model for giant magnetostrictive rod and coil optimization analysis. Nanotechnol. Precis. Eng. **12**(2), 85–90 (2014)
12. Gao, X., Liu, Y., Pei, Z.: Optimization and design for magnetic circuit in giant magnetostrictive actuator. J. Harbin Inst. Technol. Univ. **48**(9), 145–150 (2016)

13. Shuying, C., Bowen, W., Rongget, Y.: Dynamic model with hysteresis nonlinearity for a giant magnetostrictive actuator. Proc. CSEE **23**(11), 145–149 (2003)
14. Jiles, D.C., Atherton, D.L.: Theory of magnetization process in ferromagnets and its application to magnetic mechanical effect. Phys. D Appl. Phys. **17**, 1265–1281 (1984)
15. Jiles, D.C., Atherton, D.L.: Theory of ferromagnetic hysteresis. J. Magn. Magn. Mater. **6**(2), 48–53 (1986)
16. Calkins, F.T., Smith, R.C., Flatau, A.B.: Energy based hysteresis model for magnetostrictive transducers. IEEE Trans. Magn. **36**(2), 429–439 (2000)
17. Jiles, D.C.: Frequency dependence of hysteresis curves in conducting magnetic materials. J. Appl. Phys. **76**(10), 5849–5855 (1994)
18. Jiles, D.C.: Dynamics of domain magnetization and the Barkhausen effect. Czech J. Phys. **50**(8), 893–924 (2000)
19. Gao, X., Liu, Y., Pei, Z.: Minor hysteresis loop dynamic Jiles-Atherton model in giant magnetostrictive actuator. J. Beijing Univ. Aeronaut. Astronaut. **42**(12), 2648–2653 (2016)
20. Wenbin, W.: Machinerys Handbook, pp. 7–30. China Machine Press, Beijing (2004)
21. Liu, Y., Gao, X., Li, Y.: Giant magnetostrictive actuator nonlinear dynamic Jiles–Atherton model. Sens. Actuators A Phys. **250**, 7–14 (2016)